ADVANCED MATERIALS
www.advmat.de

www.MaterialsViews.com

Emergent Functionality and Controllability in Few-Layer Metasurfaces

Hua Cheng, Zhaocheng Liu, Shuqi Chen, and Jianguo Tian**

Recent progress in metamaterial research has successfully exceeded the limitations imposed by conventional materials and optical devices, enabling the manipulation of electromagnetic waves as desired. The distinct characteristics and controlling abilities of metamaterials make them ideal candidates for novel photonics devices not only in traditional optics but also for biological detection, medical science, and metrology. However, the controllability and functionality of both single-layer metasurfaces and bulk metamaterials are not sufficient to meet the requirements of emerging technologies; hence, new solutions must be found. As such technologies advance, new functionalities will emerge as different or identical single-layer metasurfaces are combined. Thus, innovation in few-layer metasurfaces will become an increasingly important line of research. Here, these metasurfaces are classified according to their functionalities and the few-layer metasurfaces that have been proposed up to now are presented in a clear sequence. It is expected that, with further development in this area, few-layer metasurfaces will play an important role in the family of optical materials.

1. Introduction

To overcome the physical limitations imposed by natural materials and to direct light in unprecedented ways and with greater precision, researchers are looking for artificial substitutes for conventional natural materials. Metamaterials, which are assembled from multiple individual elements composed of conventional materials, but usually constructed into repeating patterns, are an important family of such artificial materials within the framework of Maxwell's electromagnetic theory. The distinct properties of metamaterials notably helped to experimentally verify the negative index,[1] which, in 1967, was only a seemingly unprovable impractical theory published by Veselago.[2] These negative-index materials additionally permitted the creation of superlenses that can greatly improve optical resolution beyond that achieved by conventional optical lenses, and close to the limits predicted by Abbe.[3] Metamaterials have also exhibited remarkable properties in applications, such as invisibility cloaks,[4–6] strong-chiral materials,[7] zero-index materials,[8] and optical black holes,[9,10] operating from microwave wavelengths to visible wavelengths, opening up a new research field and demonstrating their enormous potential in a range of applications.

Recently, planar metasurfaces have attracted a great deal of attention. In contrast to three dimensional (3D) bulk metamaterials, metasurfaces, which are capable of abruptly changing the state of light, contain resonators of various shapes or structures arranged periodically on 2D surfaces. These planar metasurfaces, which have thicknesses less than or similar to the wavelength of light, have shown extraordinary abilities to control the intensity and momentum of light.[11–13] Single-layer metasurfaces have been successfully proven to be feasible for use in engineering the phase, amplitude, and polarization of light. For first time, the generalized Snell law was proposed and experimentally demonstrated on metasurfaces with arrays or V-shaped antennas.[14–16] Subsequently, numerous applications based on single-layer metasurfaces, such as 2D ultrathin lenses,[17,18] high-resolution holograms,[19] vortex-beam generators,[20,21] refractive quarter-wave plates,[22] demonstration of the spin Hall Effect of light,[23–26] and PT symmetry breaking,[27] have been proposed and achieved.

Although great progress in the field of single-layer metasurfaces has been made, some problems remain. Because a single-layer metasurface offers only limited interaction between light and scatterers (i.e., the resonators or antennas), the major energy cannot be controlled, and the efficiency is lower than that required for practical applications. The limited control can be surmounted with 3D metamaterials, in which light interacts continuously with the metamaterials and the wavefront can be finely modified. However, at the same time, light typically must exchange energy with each meta-molecule, and, if the material of the meta-molecules incurs non-ignorable losses, a large amount of energy will be wasted to heat loss. Moreover, the fabrication of artificial bulk metamaterials is a problem when the volume of the bulk is large (compared to the wavelength) and each molecule has a complex shape.

As shown in **Figure 1**, few-layer metasurfaces provide an alternative way to overcome the drawbacks of both single-layer metasurfaces and bulk metamaterials. Compared with single-layer metasurfaces, the extra effects induced by multiple layers dramatically improve the applicability of few-layer systems. The

Prof. H. Cheng, Z. Liu, Prof. S. Chen, Prof. J. Tian
Laboratory of Weak Light Nonlinear Photonics
Ministry of Education
School of Physics and Teda Applied Physics Institute
Nankai University
Tianjin 300071, China
E-mail: schen@nankai.edu.cn; jjtian@nankai.edu.cn

DOI: 10.1002/adma.201501506

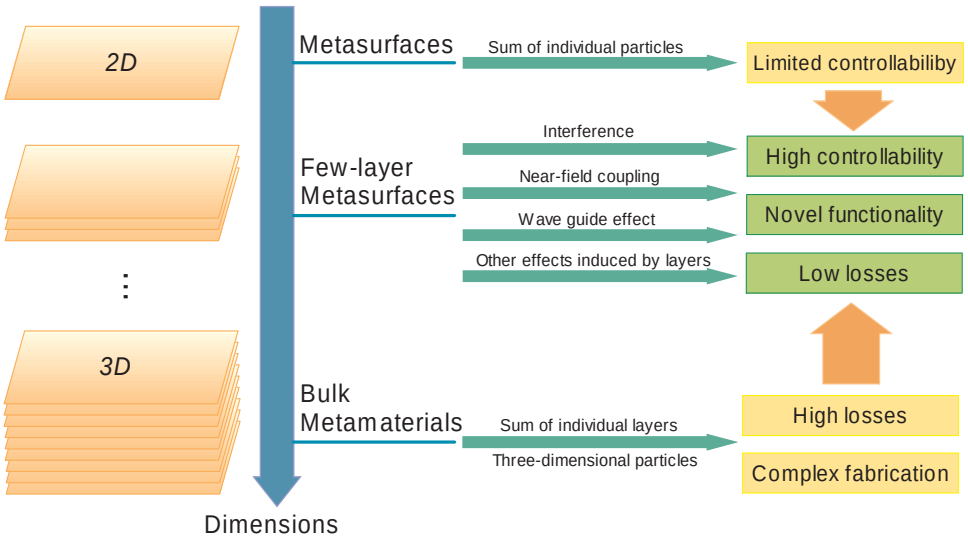

Figure 1. Schematic illustration of different metamaterials and their properties induced by various effects. The functions of metasurfaces with two dimensions are usually the sum effects of the individual resonator on the surface, offering limited controllability, whereas bulk metamaterials with three dimensions have the function caused by the sum of individual layers or large 3D particles, exhibiting high losses and requiring a complex fabrication process. Few-layer metasurfaces, falling in between these two metamaterials, usually have emergent effects (such as interference and near-field intensification) and contribute to the development of new-type metasurfaces with high controllability, novel functionality, and low losses.

interference and near-field coupling between layers ensure that the energy can be strongly redistributed and can interact with the structures. The total function is no longer a simple superposition between each original layer but, rather, an emergent function with higher controllability and efficiency. Furthermore, the multiplication of layers can provide more degrees of freedom to manipulate the propagation, polarization, and phase amplitude of light. When compared with bulk metamaterials, few-layer systems have far fewer dimensions, which makes the fabrication processes readily achievable; in addition, owing to the immediate interaction between the light and the surface with this optically thin system, the loss of light energy is no greater than in bulk metamaterials. Aside from the merits described above, a great number of new phenomena and applications might be possible if other materials can be introduced into few-layer metasurface systems. Hence, few-layer metasurfaces provide a remarkable solution to the current difficulties in metamaterials, and are promising technologies for novel functional photonics devices and applications.

Natural materials are formed of clusters of atoms and molecules. Each atom or molecule has its own properties, such as energy level and radius, but a regular combination of single or multiple types of molecules will create novel properties that are never found in single molecules. The same principle holds for single-layer metasurfaces. The basic unit of a metasurfaces is the meta-molecule, which is made of resonators or antennae of various shapes. Each meta-molecule has its own characteristics, such as the resonating mode, radiation, and absorption spectrum. New properties will emerge as a result of the careful arrangement of sufficient meta-molecules on a surface. Similarly, it is easy to understand why few-layer metasurfaces, functioning with identical or distinct layers, possess outstanding characteristics compared with single-layer metasurfaces. In view of the distinct properties of few-layer metasurfaces, it is necessary to classify and summarize the recent progress that has been made in this area. To this end, we present here a few particularly exciting research achievements that have recently come to prominence in the field of few-layer metasurfaces and hold the potential to further push the boundaries of this field. In Section 2, we summarize two universal approaches to improve the functionality of single-layer functional metasurfaces by introducing auxiliary metasurfaces, which involve both interference and near-field coupling effects between the functional and auxiliary metasurfaces. In Section 3, we discuss several recently introduced paradigms of total control over the phase and amplitude of light, which represent novel methods to control the wavefront of light without existing normal transmitted light, and discuss new theories for the design of ultrathin optical devices that can realize functions associated with polarization manipulation. Unlike the metasurfaces described in Section 2, which can control the amplitude and phase of light, this section discusses few-layer metasurfaces whose controlling properties are realized by the combination of all layers, producing more degrees of freedom and controlling parameters. Finally, with the asymmetrical properties of few-layer metasurfaces presented in Section 4, we provide a few examples of applications that can completely and asymmetrically manipulate polarization. The overall discussion is based not only on metallic metasurfaces but also on dielectric and graphene materials. The newly selected materials show a competitive capability in resolving some of the remaining difficulties in metallic metamaterials.

2. Major Improvements in Function and Efficiency

Single-layer metasurfaces have certain properties, such as polarization conversion and phase-amplitude control; however, these functions are usually incomplete or inefficient because of the limited interaction between light and the functional

metasurfaces. In addition to the high loss of metal associated with these materials, total polarization conversion and phase-amplitude control are not possible. To resolve this dilemma, we can optimize the functionality of the original metasurfaces by adding one or two auxiliary metasurfaces close to the functional metasurfaces. The auxiliary metasurfaces can usually be regarded as reflectors, used to repeatedly enhance the interaction between light and the functional metasurfaces and the resonance of the scatters.

Interference induced by layers is one of the most effective approaches to trapping light between layers and improving the interaction between light and the metamaterial. Chen et al. first demonstrated the viability of this method through the realization of a two-layer antireflection-coating metamaterial.[28] At the interface of the two media, both reflection and refraction occur when light propagates from one medium to the other, and the amplitudes of reflection and transmission are determined by Fresnel's Law. Traditionally, to eliminate reflection in a desired waveband, the structures of the metasurface must be designed on the interface to change the permittivity ε and permeability μ so that an impedance mismatch of the two media can be alleviated. However, thus far, this general concept of metamaterials still suffers from high energy losses. Instead of a single-layer coating, the two-layer antireflection configuration, with arrays of gold electric split-ring resonators (SRRs) and a gold mesh spaced by polyimide, as shown in **Figure 2**a, dramatically improves the transparency of the interface to 90% and suppresses the reflectance to 0.32% at 1.2 THz at the air–GaAs interface. This improvement is due to the interference of light itself between two layers, as shown in Figure 2b, rather than a magnetic response.[29] The overall reflection $\tilde{r}$ and transmission $\tilde{t}$ are then superpositions of the multiple reflections and transmissions resulting from the SRRs and mesh surfaces. Figure 2c also experimentally displays the excellent capacity of a two-layer antireflection configuration to alleviate reflectance at a tilted incidence in both transverse electric (TE) and transverse magnetic (TM) polarizations.

A similar scheme can be applied to the conversion of linearly polarized light. A nanorod itself is a scatterer that can generate cross-polarized light when the incident polarization direction is 45° with respect to the long axis of the nanorod. However, single-layer arrays of nanorods have limited efficiency for converting the original polarization to cross-polarization; in addition, they cannot completely abolish the original polarization component. However, by adding auxiliary surfaces beside the rod arrays, high-performance polarization conversion can be achieved across a very broad bandwidth.[30] Figure 2d provides an illustration of the basic unit for a three-layer polarization-conversion metamaterial. The functional structures, nanorods, are sandwiched between two orthogonal metal gratings attached by polyimide. A series of reflections occurs between the gratings, where the reflected energy interacts with the nanorods repeatedly. The high cross-polarized transmission shown in Figure 2e demonstrates the interferometric mechanism. This method can be universally applied to linearly polarized conversion systems. Figure 2f illustrates the arrays of resonators realizing cross-polarized anomalous refraction. With the help of the two gratings, co-polarized light repeatedly interacts with the phase gradient structure, and the converted cross-polarized light completely transmits through and forms the anomalous refraction. As shown in Figure 2g, high-intensity anomalous refractions (whose maximum intensity is 0.6 at 1.4 THz) with cross-polarization are detected from 0.8 THz to 1.8 THz, but no normal refractions are found.

Despite the increased efficiency for transmission, the diffraction efficiency could be even more fully optimized in reflection by including a metal substrate under functional structures. The metal substrate here usually serves as a reflector to reflect light to further couple with the functional structure, exhibiting the same inference mechanism as described above.[31–34] However, when the spacer between the structure and the metal substrate d narrows (e.g., $d = \lambda_{\text{eff}}/10$, where λ_{eff} is the effective wavelength in the spacer), another factor, called the gap-plasmon, must be taken into account because the coupling between the structure and the metal becomes influential.[35,36] For a series of different-sized nanorods with no metal ground plane, the excited phase retardation cannot reach 2π when the stimulated amplitudes are kept equal. However, the coupling of metal with the rods would greatly strengthen the resonance of the rods and make the total phase retardation range achievable. For instance, co-polarized anomalous reflection based on a gap-plasmon with high intensity could be realized, as shown in **Figure 3**a.[37] When changing the length and width of each rod (or patch, more exactly) at the same time, as shown in Figure 3b, phase-amplitude manipulation with higher precision can be achieved.[38,39] Figure 3c presents the effect of a 1D reflective focusing flat mirrors in a visible waveband made of Au patches with the appropriate aspect ratio accompanied by the metal substrate. The reflectance can be improved to 80% theoretically and 50% experimentally. Interestingly, because of the strong coupling, the amplitude is no longer a difficult obstacle when we select the appropriate structure geometry for phase control. It is feasible to find appropriate metal patches, whose two resonant modes in two orthogonal axes have the required phase difference to realize a bi-reflection or wave plate.[40–43] Other conventional applications that require phase manipulation with high efficiency, such as creating high-resolution holograms, are also feasible with this method.[44]

The efficiency limitation that results from Ohmic losses can be further overcome if we use other high-index dielectric materials as the basic unit for designing the metasurface; high losses can be dramatically suppressed because of Mie resonance stimulated in these dielectric materials.[46] A 98% polarization conversion is achieved in reflection if the silicon nanorods are set above a silver substrate separated by poly(methyl methacrylate) (PMMA), as shown in Figure 3d.[45] The efficiency of converting polarization reaches close to 1 from 1400 nm to 1650 nm, as presented in Figure 3e. In this case, the metal (silver) substrate is reported to serve only as the reflector. What makes the dielectric metasurface more applicable is the distinct resonance modes excited in rods with different aspect ratio. Phase control from 0 to 2π for a cross-polarized wave with extremely high intensity (theoretically up to 94.5%) can be readily realized. This property has been demonstrated in vortex-beam generation, as shown in Figure 3f, where the interference pattern of a vortex beam generated by a dielectric metasurface (with topological charge $l = 1$) and co-polarized Gaussian beam are presented. Recently, Lin et al. proposed another technique

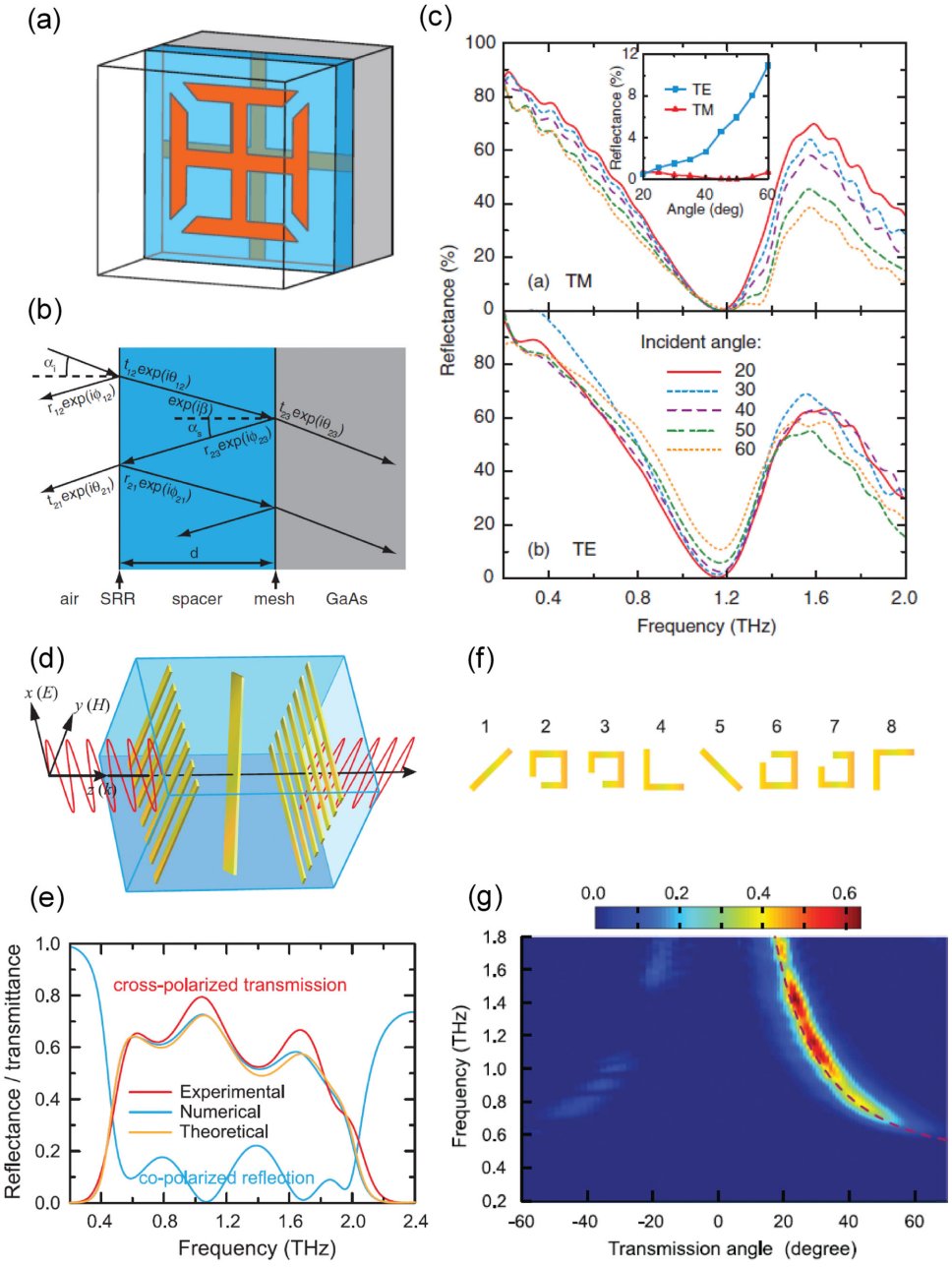

Figure 2. a) Schematic design of the two-layer metamaterial antireflection coating. The basic cell is composed of an SRR and gold mesh separated by polyimide. b) Illustration of the interference model of the metamaterial antireflection coating and associated variables. c) Experimental results of reflectance spectra from the metamaterial-coated GaAs surface for transverse magnetic (TM)- and transverse electric (TE)-polarized incident THz radiation at various incidence angles. Inset: Angular-dependent reflectance at the antireflection frequency. a–c) Reproduced with permission.[28] Copyright 2010, American Physical Society. d) Schematic of the unit cell of the three-layer metamaterial linear polarization converter, in which a normally incident *x*-polarized wave is converted into a *y*-polarized wave. The cut-wire array is covered by gold grating wires in polyimide. e) Cross-polarized transmittance obtained through experimental measurements, numerical simulations, and theoretical calculations. Also shown is the numerically simulated co-polarized reflectance. f) Resonator array super-unit-cell with the function of generating anomalous cross-polarized refraction. g) Experimentally measured cross-polarized transmittance as a function of frequency and angle for the resonator array shown in (f) sandwiched by two gold gratings. The dashed curve is the theoretically calculated frequency-dependent bending angle. d–g) Reproduced with permission.[30] Copyright 2013, American Association for the Advancement of Science.

that uses the dielectric on a gradient metasurface for highly efficient transmission,[47] but this outstanding work operates on a mechanism totally different from Mie resonance and is thus outside the scope of this article. Graphene metasurfaces constitute another branch in this area. To increase the interaction of light and graphene, it is feasible to add metallic auxiliary

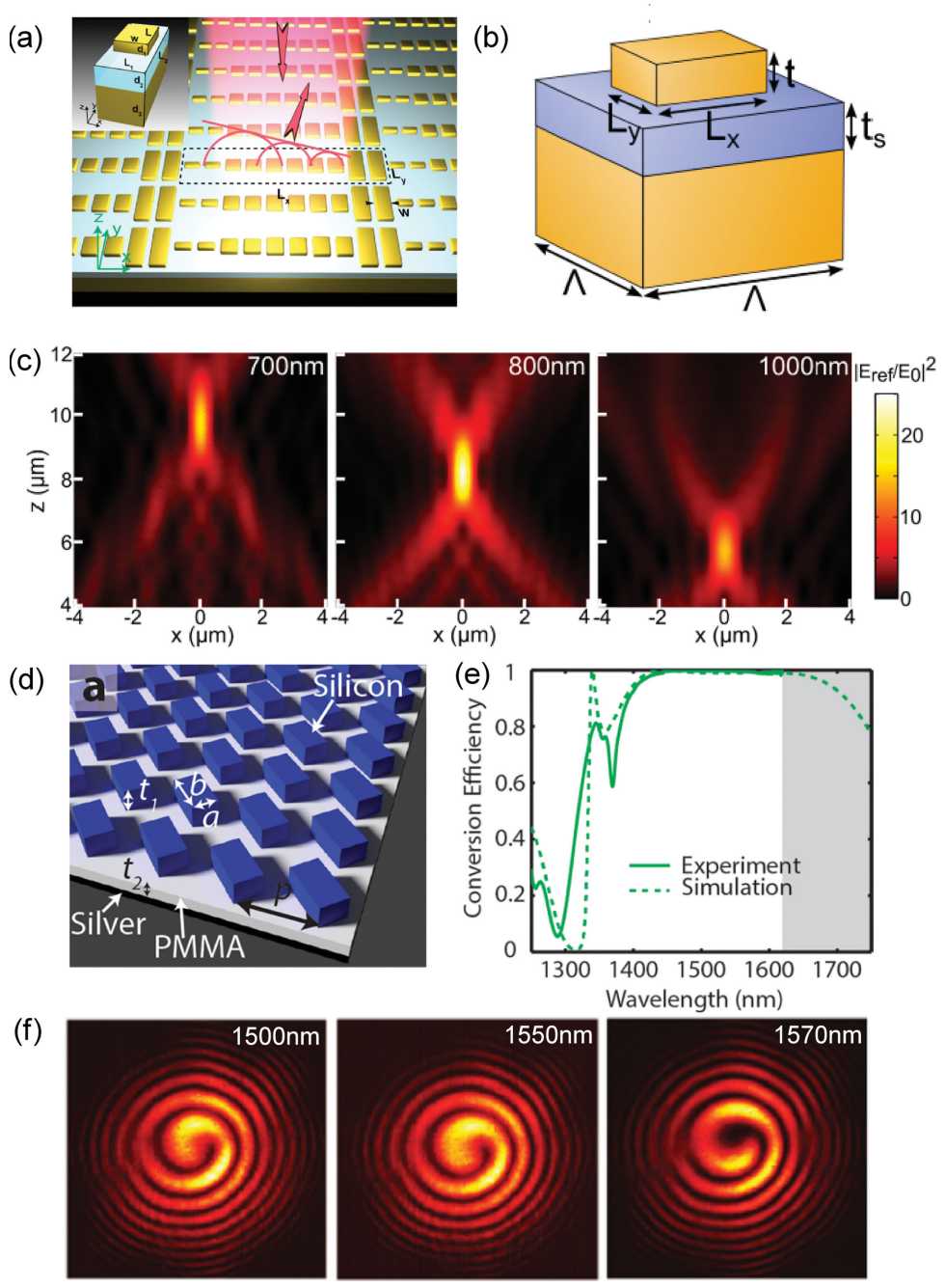

Figure 3. a) Schematic of designed anomalous-reflection metasurface with a unit cell (inset) consisting of a Au nanorod (yellow) and a continuous Au film (yellow) separated by the MgF_2 spacer (blue). A super cell of the sample (region surrounded by dashed line) consists of 5-group unit structures with different lengths but the same width. All the structures in the super cell reflect incident light with the same amplitudes but gradient phase. Reproduced with permission.[37] Copyright 2012, American Chemical Society. b) An optimized model of amplitude–phase control in reflection. The desired amplitude and phase can be precisely achieved by changing both the length L_x and width L_y of the rod. c) The intensity mA near focus of the focusing mirror made up of cells shown in (b) at wavelengths of 700 nm, 800 nm, and 1000 nm. The phase profile of the metasurface is set to be hyperboloid. b,c) Reproduced with permission.[38] Copyright 2013, American Chemical Society. d) Schematic of the polarization conversion metasurface made of dielectrics: the silicon resonators array and metal substrate are spaced by PMMA. The linearly polarized incident light with polarization angle 45° with respect to the resonators will be totally reflected to the cross-polarized light. e) Polarization conversion efficiency of the metasurface presented in (d) when each resonator has the size $a = 250$ nm and $b = 500$ nm in a period $p = 650$ nm. f) Interference pattern of a vortex beam generated by a dielectric metasurface (with topological charge $l = 1$) and co-polarized Gaussian beams at 1500 nm, 1570 nm, and 1570 nm. The phase profile and amplitude distribution of the metasurface are determined by different-sized silicon resonators. d–f) Reproduced with permission.[45] Copyright 2014, American Chemical Society.

metasurfaces beside the graphene metasurfaces.[48,49] Dynamic control of electromagnetic waves, including their polarization and transmission, thus can be efficiently achieved.

3. Total Control of Phase and Amplitude

Control of the phase and amplitude of light has been realized by a single-layer metasurface. Optical antennae of various shapes have been utilized to control the co-polarized and cross-polarized wavefront. However, a single-layer metasurface itself cannot achieve highly efficient control while eliminating normally transmitted light (i.e., light that is not controlled). This limitation arises mainly because the single interface radiates equally on both sides of the metasurface, and the existence of a reflection drastically decreases the efficiency of transmission. Even if impedance matching could be achieved (resulting in no reflection occurring), the degree of freedom to control the phase would not be sufficient. Recently, several new types of few-layer metasurfaces, each based on a novel mechanism, have successfully overcome these drawbacks. In addition to the control of phase and amplitude, polarization can also be manipulated on some metasurfaces. The universality of these mechanisms would further guide us to a great number of efficient structures and applications.

The first type of few-layer metasurface is made up of cascaded layers of structures, schematically shown in **Figure 4**a,b.[50–52] Each layer has a basic unit containing a patch in the center and a wire grid outlining the unit. Equivalently, the unit is an *LC* circuit that is induced by electric inertia and the wire grid and whose capacitance is created by the patch. Consequently, the structure has the admittance Y_S. It is theoretically possible to change the phase of the transmitted field by adjusting the Y_S value of the metasurfaces while at the same time maintaining its high efficiency. However, single-layer metasurfaces cannot achieve this goal, which motivates cascading multiple sheet admittances with dielectric spacers separating them. Three layers have been proven to be the minimum number of layers to cover the 2π phase range. However, the use of more layers improves the controlling effect. If the structure of each layer is isotropic, it changes only the phase of the wavefront, and the polarization of incidence is not affected. Figure 4c,d present the anomalous refraction realized by a three-sheet isotropic metasurface. Unusually, normal refractive light and reflective light are not found at the designed wavelength, and the transmitted polarization is maintained the same as that of the incident light. Furthermore, if the structure is anisotropic, the polarization can be simultaneously manipulated because the phase delays in the two orthogonal axes are no longer equal.[52] This structure offers a universal concept for designing metasurfaces, since any device can be produced by designing the phase and polarization of controlled light, such as wave plates and superlenses. Meanwhile, this kind of cascaded metasurfaces requires several lithography steps; therefore, they are as practical as most other types of metasurfaces that only incorporate a metal ground plane. In fact, highly integrated metasurfaces with multiple functions are readily achievable with this method.

The second type of few-layer metasurface is based on the excitation of surface plasmon polaritons (SPPs) on both sides of a metasurface.[53] Illustrations of this type of two-layer metasurface are shown in Figure 4e,f. Each unit contains a pair of rectangular nanoapertures embedded in SiO_2. A standing wave of SPPs, indicated by the blue and red arrows in Figure 4e,f, is created by the metal–insulator–metal (MIM) waveguide composed of two metal layers.[54,55] This waveguide mode is the crucial point for determining the phase of the transmitted light. Figure 4f presents the two-layer metasurface with lateral translation *S*. The simulated electrical pattern indicates the standing wave of SPPs. Two parameters, the length of apertures *L* and the lateral translation between the two layers *S*, mainly contribute to the full control of the phase and amplitude. In addition to the capability of totally controlling the phase and amplitude, this waveguide-stimulated metasurface has two other advantages: i) it can filter out *x*-polarized waves, leaving the purely *y*-polarized transmitted wave (polarization-dependent property), and ii) the rotation of each unit results in the transmitted light carrying an extra Berry phase for circularly polarized (CP) light. Figure 4g illustrates the manipulation of the polarization and the phase at the same time by six units that can control the phase over the 2π range. Thus, this approach is an effective way to generate a vector beam without causing a vortex. When the incident light is CP, the polarization of the transmitted light can be determined by the orientation of the aperture, and the extra phase caused by the rotation of units can be cancelled by adjusting *L* and *S*. Therefore, a vector beam can be realized by carefully arranging the geometrical sizes and orientations of the apertures on the metasurfaces. Figure 4h presents experimental far-field intensity detection with and without an analyzer after CP light passes through such a vector-beam generator. The selectivity of polarization has also been recently applied in a Berry-phase-relating metasurface,[24–26] resulting in greater degrees of freedom in the modification of phase and polarization.

The third type of few-layer metasurface applies a similar theory as the first type, and both are designed to construct the layers of *LC* circuits to steer wavefronts efficiently. However, this approach exploits another nanocircuit paradigm to realize a broad impedance range.[56] The basic nanocircuit element is composed of the composite materials shown in **Figure 5**a. The plasmon portion and dielectric portion act as nanoinductor and nanocapacitor, respectively. The impedance of each element can be tuned by the relative length of the plasmon w and the dielectric $(l - w)$.[57] A symmetric stack of three metasurfaces is utilized to sufficiently manipulate the optical transmission and, at the same time, to minimize reflection. The amplitude and phase through a periodic stack are demonstrated to be functions of building-block width in the external and internal metasurfaces, w_{out} and w_{in}, respectively. Figure 5b presents anomalous refraction generation with no normal refraction using the arrays of a basic unit made from these composite materials. This method is predicted by simulation to have an efficiency of above 75% in the infrared region, and it has a wide bandwidth as well as robustness to heat losses. Similar to the cascaded metasurfaces shown in Figure 4a, the stack metasurfaces also need several lithography steps, and thus it is just as applicable and practical as cascaded metasurfaces and metasurfaces only with a plane ground.

As the development of few-layer metasurfaces has progressed, various novel applications have been proposed. Silva et al. demonstrated a method to carry out complex mathematical operations with the third type of metasurface described above

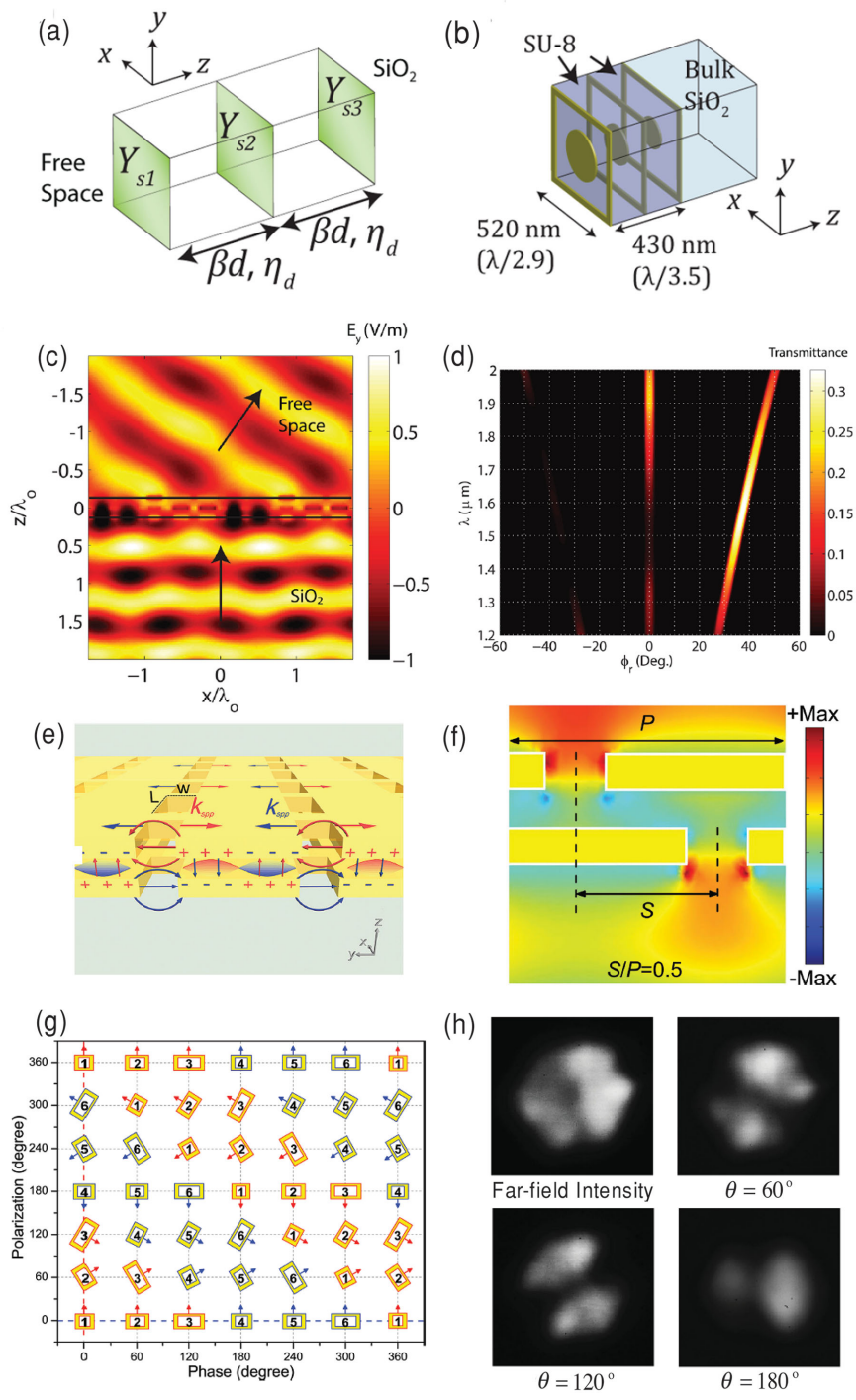

Figure 4. a) Analytic model of a unit cell comprising the three-layer metamaterial. b) Perspective view of a typical unit cell, which contains a patch in the center and a wire grid outlining the unit in each layer. c) Electric distribution of *y*-polarized anomalous light when a plane wave is normally incident from the bottom to the linear phase-gradient metasurface constituted by the units shown in (b) at the wavelength of 1.5 μm. d) Transmittance of the linear phase-gradient metasurface as function of wavelength and transmitted angle of *s*-polarized light. The transmittance of anomalous refraction is much larger than the normal refraction at the wavelength 1.5 μm. a–d) Reproduced with permission.[50] Copyright 2014, American Chemical Society. e) Schematic illustrations of the plasmonics metasurface with aligned nanoaperture pairs. The rectangular nanoapertures in the two layers have the same dimensions. The surface plasmonics standing wave is shown between the two structures, with the field and charge oscillation indicated. f) Simulated electrical pattern for nano-aperture pairs with lateral translation *S*. The surface plasmonics standing wave is a crucial factor determines the phase in transmission. g) Schematic diagram for simultaneously manipulating phase and polarization. Six basic units (marked by 1–6) cover the controlling phase from 0 to 2π with the same amplitude. The extra rotation of every unit not only determines the polarization of transmitted light but also imposes a Berry phase on it, creating a large number of degrees of freedom to control. h) Experiments with a generated vector beam after passing CP light through the sample composed of units 1–6 shown in (h) are properly rotated and arranged. The measured far-field intensity profiles representing a radially polarized beam without and with a polarizer (oriented at angle θ) intercepted before the CCD detector are displayed. e–h) Reproduced with permission.[53] Copyright 2015, Wiley-VCH.

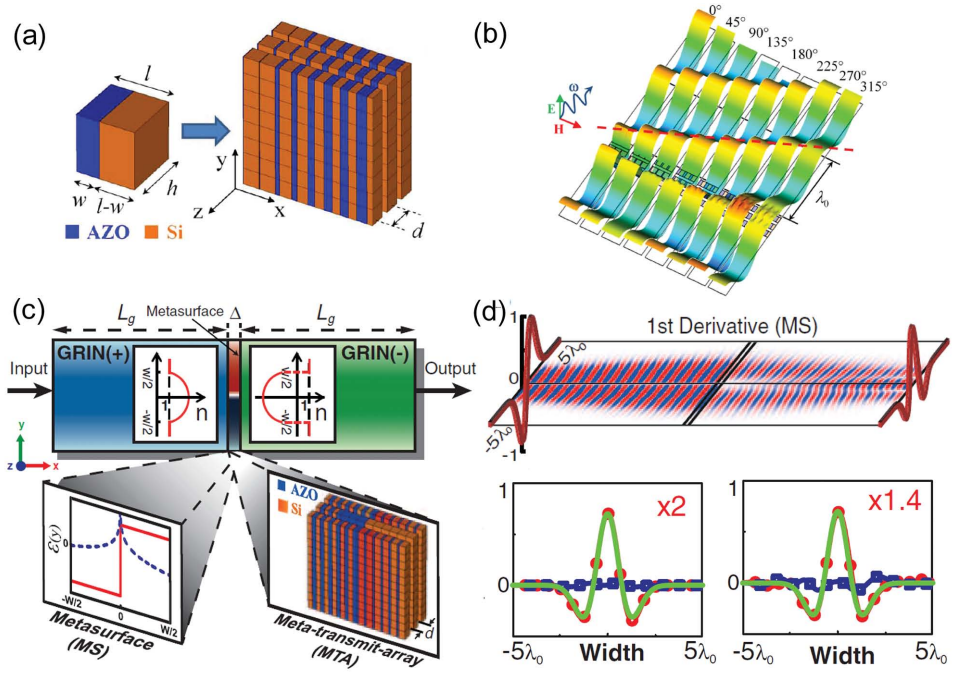

Figure 5. a) Basic building block of the metasurface (left) made of plasmonics (aluminum-doped zinc oxide) and dielectric (silicon) materials. The length and thickness of the unit cell are $l = 250$ nm and $h = 250$ nm, respectively. The width of the plasmonics w determines the impedance of each block. (right) Meta-transmit-array made of three stacked metasurfaces with a center-center distance $d = 375$ nm. b) Propagation through the stacked metasurface with linear phase gradient. The strips represent the total electric field at the same instant. Reproduced with permission.[56] a,b) Copyright 2013, American Physical Society. c) Illustration of the system that can perform mathematical operations. A properly designed metasurface is sandwiched between two GRIN structures with positive and negative parameters. d) (Top panel) Perspective view of the propagation of a wave throughout the system. The input function is shown on the left along with a snapshot of the simulation results for the z-component of the electric field throughout the metamaterial system functioning as the first differentiator. The output profile is shown on the right. (Bottom panel) Simulation results [real (red) and imaginary (blue) parts] at the output for first and second differentiation using different metasurfaces. The exact results are indicated by the green lines. Reproduced with permission.[58] c,d) Copyright 2014, American Association for the Advancement of Science.

in the Fourier domain.[58] The operation can be divided to three parts, as shown in Figure 5c, but the first and last parts involve Fourier and inverse Fourier transforms, which are realized by a graded-index (GRIN) dielectric index. Actual operations are performed by carefully designing the metasurface in the second part. If the permeability and permittivity of the metasurfaces conform with a certain relationship, differentiation, integration, and convolution can be precisely calculated. This technique requires total manipulation of the wavefront of incident light with no reflection and normal light, and thus can only be realized by few-layer metasurfaces. Figure 5d (top) presents the perspective of the propagation of a wave throughout the first-order differentiator, in which the input function is shown on the left and the output is shown on the right. Figure 5d (bottom) gives two examples of results from the first- and second-order differentiators along with the exact outcomes for comparison. The concept of mathematical metamaterials describes the possibility of highly compact, potentially integrable architectures within much smaller volumes, ensuring controlled manipulation and processing of the incoming signal. With the powerful controllability of the phase and amplitude, permeability, and permittivity of light, it is also expected that few-layer metasurfaces will have other promising applications, not only as conventional phase-controlling devices for applications such as the generation of an Airy beam[59,60] and wavefront coding,[61] but also in novel concepts such as coding metamaterials and digital metamaterials.[62,63]

4. Interesting Control of Polarization and Propagation

Few-layer metasurfaces have many more functionalities than single-layer metasurfaces. The extra effects induced by the interaction between the layers provide great contributions to novel functions and applications. One such contribution is the manipulation of the propagation direction and polarization based on the asymmetric geometry of the structure. Generally speaking, the asymmetric structures in each layer have a linear effect on the polarization of the incident wave if the layers are not extremely close.[64] The matrix analysis is available under these conditions, and many novel effects on light can be readily predicted. Because the commutative law is not commonly established in the matrix, the asymmetry can easily be found in few-layer structures. At the same time, the interference between the layers enables other optimizable parameters to enhance the transmittance or reflectance. Thus, we review below some distinct works in this field.

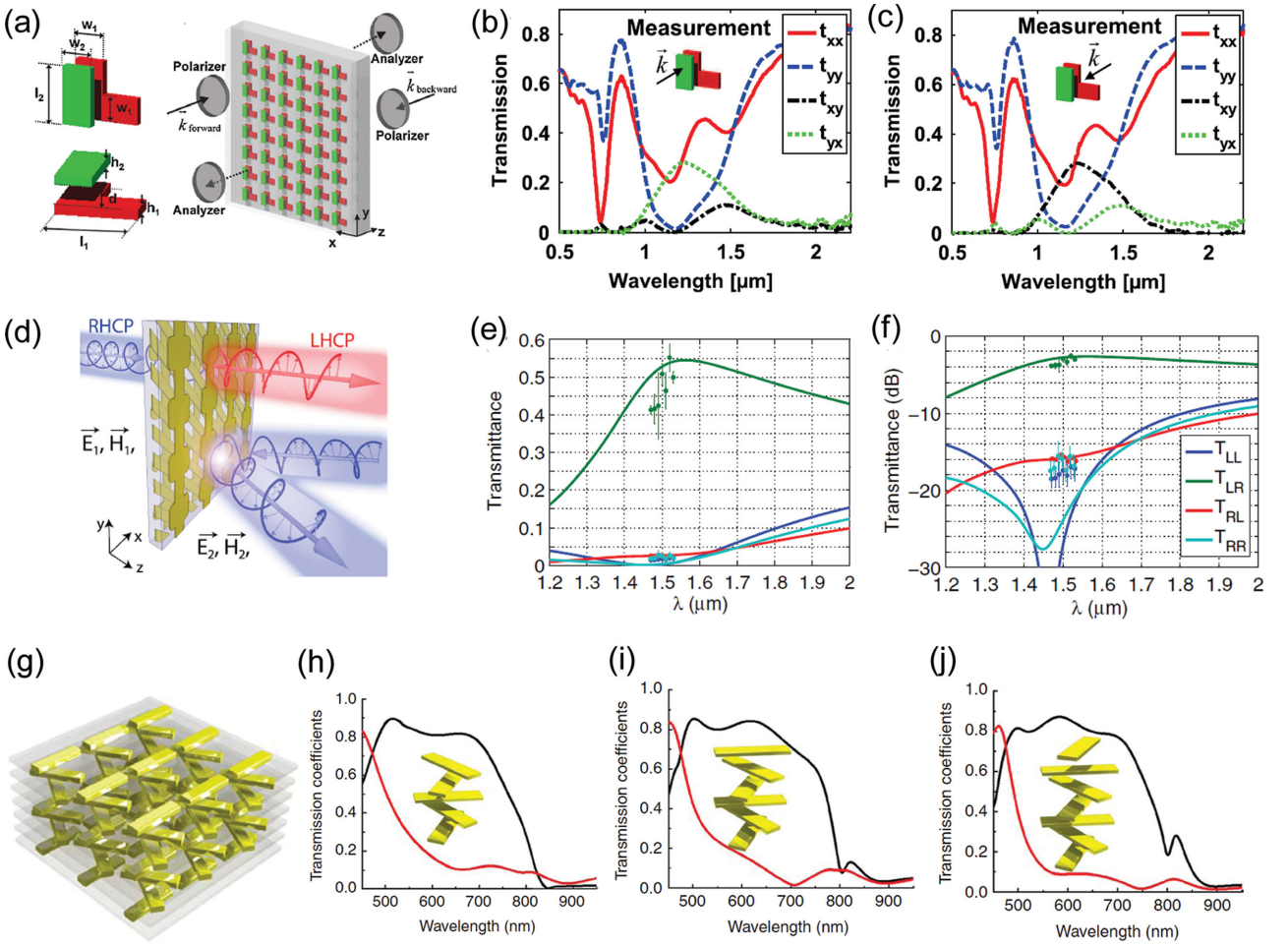

Figure 6. a) (Left) Two sketches of the two-layer metamaterial unit cell, containing an L-shaped particle and a nanowire, from different perspectives. (Right) Schematic of total metamaterials and the setup for detecting the asymmetrical transmission. b,c) Measured squared moduli of the four *T*-matrix components of the metamaterials forward (*k*-vector is directed in the positive *z* direction) and backward (*k*-vector is directed in the negative *z* direction), respectively. a–c) Reproduced with permission.[65] Copyright 2010, American Physical Society. d) Illustration of the asymmetric circular polarizer made up of three-layer metallic structures. The RCP light from region 1 is converted to LCP light in region 2, whereas RCP light from region 2 is completely reflected. e,f) Measured and simulated Jones matrix of the metasurface on linear and logarithmic scales, respectively. The solid lines correspond to simulation, and the circles correspond to measurements. d–f) Reproduced with permission.[66] Copyright 2014, American Physical Society. g) Illustration of a pair of stacked metamaterials with rotational twist θ and separation distance d. h–j) Transmittance of LCP and RCP waves through a stack of rotated metasurfaces by increasing the number of layers. The number of layers increases from two to seven, with the insets illustrating one unit cell of the corresponding twisted metamaterial slab along the direction of propagation. g–j) Reproduced with permission.[67] Copyright 2012, Nature Publishing Group.

The first observation of asymmetrical transmission for linearly polarized light was made by Menzel et al.[65] For a nanostructure, the transmission matrix for forward transmission is:

$$T^f = \begin{bmatrix} A & B \\ C & D \end{bmatrix} \quad (1)$$

where *A*, *B*, *C*, and *D* are transmission coefficients. This expression is applicable in any orthogonal basis (e.g., linearly polarized light or circularly polarized light). Applying the reciprocity theorem, the transmission matrix for backward propagation can be derived as:

$$T^b = \begin{bmatrix} A & -C \\ -B & D \end{bmatrix} \quad (2)$$

The asymmetric transmission can be observed only when $B \neq C$. This prerequisite is difficult to satisfy in a single-layer metasurface on the basis of linearly polarized light. To break the symmetry of the transmission, another layer must be added. The designed structure with strong anisotropy is shown in **Figure 6**a. The first layer is composed of arrays of L-shaped antennae, and the second one of nanorods only. If we denote the transmissions of the L-shaped-layer and nanorod-layer as:

$$T_1 = \begin{bmatrix} a & b \\ b & d \end{bmatrix} \quad (3)$$

$$T_2 = \begin{bmatrix} e & 0 \\ 0 & f \end{bmatrix} \quad (4)$$

Then the total transmission can be deduced:

$$T = \begin{bmatrix} ae & bf \\ be & df \end{bmatrix} \quad (5)$$

where the two coefficients $B = bf$ and $C = be$ are not necessarily equal. It is the nanorods here that provide the asymmetry to cause the total effect of asymmetrical transmission. The asymmetry of the few-layer metasurface for linearly polarized light is demonstrated, as shown in Figure 6b,c, where the transmission coefficients t_{xy} and t_{yx} are reversed at forward and backward incidences. As far as the circularly polarized light is concerned, it is much easier to observe the asymmetrical transmission. With circularly polarized light, B and C are $ae - df - i(be + bf)$ and $ae - df + i(be + bf)$, respectively. The natural inequality determines the impossibility of making the transmittances equal under forward and backward conditions. Experiments have fully proved this point. Other structures with multiple layers can also realize asymmetry if the geometry and orientation of the structures in each layer are carefully arranged.[68]

After the observation of asymmetrical transmission in few-layer metasurfaces, control of the polarization and propagation of waves on these metasurfaces has been developed to meet the demands of photonic nanodevices. Bi-anisotropic metasurfaces are one of the focuses of this research because of their promising applications in optical switches and diodes. Bi-anisotropic characteristics have been successfully found in two-layer metasurfaces.[69] However, Pfeiffer et al. proposed a universal method to design metasurfaces with at least three layers in order to realize any desired asymmetrical functions.[66] Figure 6d shows a proposed three-layer structure that can convert the right circularly polarized (RCP) light into its opposite helicity, left circularly polarized (LCP), when propagating forward, while preventing backward-propagating RCP light. The structure is designed by first solving the admittance of each layer numerically and then finding specific structures to realize the admittance. Although the bi-anisotropic function can be fulfilled by arranging quarter-wave plates and polarizers appropriately,[70] this designed metasurface is mostly attributed to the electric/magnetic response and the collective impact between the layers. This behavior can be understood by the fact that metallic structures in a single layer cannot create perfect polarizers and wave-plates. Figure 6e,f show the performance of this material's strongly asymmetrical property, in which a maximum transmission of 0.55 is achieved. Due to the universality of this method, it has been proven possible to design optical devices (e.g., polarization rotators and wave-plates) at millimeter-wave and microwave frequencies.[71,72] This material is thus also a promising candidate to fill the terahertz gap and thereby to achieve high performance.

Few-layer metasurfaces also provide an alternative to readily fulfill the function of 3D structures in circular polarization control. Zhao et al. proposed the approach to realize a circular polarizer by stacked metasurfaces.[67] It was reported that one can use the 3D chiral structure to remove a certain of helicity for the incident wave,[73–75] but the fabrication is rather difficult. However, the twisted structure shown in Figure 6g has a similar effect and has a much simpler design. The basic unit is composed of stacked nanorods with a rotation angle $\theta = 60°$ in the propagation direction. It has been shown, according to Figure 6h–j, that the distinct effect for two opposite helicities becomes increasingly influential as the layers increase. Unlike cholesteric liquid crystals or helicoidal materials, the operation of a twisted metasurface is based on the strong resonant anisotropy at the metasurface level over a subwavelength period, resulting in a drastically larger bandwidth. Moreover, it has been shown that the undesired misalignment between layers only has a slight influence on the overall selectivity effect, and thus it releases the fabrication requirements in practical applications.

Asymmetrical properties are difficult to realize on a single-layer metasurface, and the total control of polarization and propagation is inaccessible with a one-layer structure. Despite the methods we have reviewed above, there have been many exciting efforts to realize asymmetrical manipulation and polarization control.[76] With improvements in precision and fabrication techniques, a greater number of effective and even dynamically controllable novel-functional few-layer metasurfaces are achievable.

5. Conclusions and Outlook

In this article, we have presented and discussed a few of the highly promising work that has been carried out regarding few-layer metasurfaces. With a multiple-layer system, the functional single-layer metasurfaces can be further optimized, and, meanwhile, new functions and phenomena may also emerge. Owing to their wavelength-scale dimensions, ease of fabrication, and general applicability for all wavelengths, few-layer metasurfaces with prominent properties have applications in both traditional-functional optical-device improvement and novel-functional integral-systems development. The ready availability of composite multiple functions opens up more directions in nanophotonics and materials research. However, research on few-layer metasurfaces is just beginning. Research on physical layers, such as achieving the control of light using differently structured metasurfaces, and on applications for these materials, such as mathematical operation and coding metamaterials, is rapidly progressing. We predict that, with more materials, such as dielectric, graphene, and quantum dots being applied to few-layer metasurfaces, the functionality of these materials will continue to expand. Recent advances in 2D soft nanomaterials,[77] including $B_xC_yN_z$ nanosheets and 2D supermolecular organic nanostructures, and morphology genetic materials,[78] might also offer a new research direction for few-layer metasurfaces. Overall, the great potential of metamaterials is only beginning to be revealed.

Acknowledgements

This work was supported by the National Basic Research Program (973 Program) of China (2012CB921900), the Chinese National Key Basic Research Special Fund (2011CB922003), the Natural Science Foundation of China (61378006 and 11304163), the Program for New Century Excellent Talents in University (NCET-13–0294), the International

Science & Technology Cooperation Program of China (2013DFA51430), the Natural Science Foundation of Tianjin (13JCQNJC01900), the National Science Fund for Talent Training in Basic Sciences (J1103208), and the 111 project (B07013).

Received: March 30, 2015
Revised: July 2, 2015
Published online: August 12, 2015

[1] R. A. Shelby, D. R. Smith, S. Schultz, *Science* **2001**, *292*, 77.
[2] V. G. Veselago, *Sov. Phys. Uspekhi* **1968**, *10*, 509.
[3] J. B. Pendry, *Phys. Rev. Lett.* **2000**, *85*, 3966.
[4] A. Alù, E. Nader, *Phys. Rev. E* **2005**, *72*, 016623.
[5] J. B. Pendry, S. David, R. S. David, *Science* **2006**, *312*, 1780.
[6] D. Schurig, J. J. Mock, B. J. Justice, S. A. Cummer, J. B. Pendry, A. F. Starr, D. R. Smith, *Science* **2006**, *314*, 977.
[7] E. Plum, J. Zhou, J. Dong, V. A. Fedotov, T. Koschny, C. M. Soukoulis, N. I. Zheludev, *Phys. Rev. B* **2009**, *79*, 035407.
[8] E. J. R. Vesseur, C. Toon, C. Humeyra, E. Nader, P. Albert, *Phys. Rev. Lett.* **2013**, *110*, 013902.
[9] E. E. Narimanov, V. K. Alexander, *Appl. Phys. Lett.* **2009**, *95*, 041106.
[10] S. Chen, H. Cheng, H. Yang, J. Li, X. Duan, C. Gu, J. Tian, *Appl. Phys. Lett.* **2011**, *99*, 253104.
[11] N. Yu, F. Capasso, *Nat. Mater.* **2014**, *13*, 139.
[12] N. I. Landy, S. Sajuyigbe, J. J. Mock, D. R. Smith, W. J. Padilla, *Phys. Rev. Lett.* **2008**, *100*, 207402.
[13] L. Liu, X. Zhang, M. Kenney, X. Su, N. Xu, C. Ouyang, Y. Shi, J. Han, W. Zhang, S. Zhang,*Adv. Mat.* **2014**, *26*, 5031.
[14] N. Yu, P. Genevet, M. A. Kats, F. Aieta, J. P. Tetienne, F. Capasso, Z. Gaburro, *Science* **2011**, *334*, 333.
[15] X. Ni, N. K. Emani, A. V. Kildishev, A. Boltasseva, V. M. Shalaev, *Science* **2012**, *335*, 427.
[16] F. Aieta, P. Genevet, N. Yu, M. A. Kats, Z. Gaburro, F. Capasso, *Nano Lett.* **2012**, *12*, 1702.
[17] X. Chen, L. Huang, H. Mühlenbernd, G. Li, B. Bai, Q. Tan, G. Jin, C.-W. Qiu, S. Zhang, T. Zentgraf, *Nat. Commun.* **2012**, *3*, 1198.
[18] M. Kang, T. Feng, H.-T. Wang, J. Li, *Opt. Express* **2012**, *20*, 15882.
[19] L. Huang, X. Chen, H. Mühlenbernd, H. Zhang, S. Chen, B. Bai, Q. Tan, G. Jin, K. W. Cheah, C.-W. Qiu, J. Li, T. Zentgraf, S. Zhang, *Nat. Commun.* **2013**, *4*, 2808.
[20] P. Genevet, N. Yu, F. Aieta, J. Lin, M. A. Kats, R. Blanchard, M. O. Scully, Z. Gaburro, F. Capasso, *Appl. Phys. Lett.* **2012**, *100*, 013101.
[21] L. Huang, X. Chen, H. Mühlenbernd, G. Li, B. Bai, Q. Tan, G. Jin, T. Zentgraf, S. Zhang, *Nano Lett.* **2012**, *12*, 5750.
[22] N. Yu, F. Aieta, P. Genevet, M. A. Kats, Z. Gaburro, F. Capasso, *Nano Lett.* **2012**, *12*, 6328.
[23] X. Yin, Z. Ye, J. Rho, Y. Wang, X. Zhang, *Science* **2013**, *339*, 1405.
[24] N. Shitrit, L. Yulevich, E. Maguid, D. Ozeri, D. Veksler, V. Kleiner, E. Hasman, *Science* **2013**, *340*, 724.
[25] N. Shitrit, I. Bretner, Y. Gorodetski, V. Kleiner, E. Hasman, *Nano Lett.* **2011**, *11*, 2038.
[26] K. Y. Bliokh, Y. Gorodetski, V. Kleiner, E. Hasman, *Phys. Rev. Lett.* **2008**, *101*, 030404.
[27] M. Lawrence, N. Xu, X. Zhang, L. Cong, J. Han, W. Zhang, S. Zhang, *Phys. Rev. Lett.* **2014**, *113*, 093901.
[28] H.-T. Chen, J. Zhou, J. F. O'Hara, F. Chen, A. K. Azad, A. J. Taylor, *Phys. Rev. Lett.* **2010**, *105*, 073901.
[29] H.-T. Chen, *Opt. Express* **2012**, *20*, 7165.
[30] N. K. Grady, J. E. Heyes, D. R. Chowdhury, Y. Zeng, M. T. Reiten, A. K. Azad, A. J. Taylor, D. A. R. Dalvit, H.-T. Chen, *Science* **2013**, *340*, 1304.
[31] Q. Lévesque, M. Makhsiyan, P. Bouchon, F. Pardo, J. Jaeck, N. Bardou, C. Dupuis, R. Haïdar, J. L. Pelouard, *Appl. Phys. Lett.* **2014**, *104*, 111105.
[32] Y. Li, J. Zhang, S. Qu, J. Wang, H. Chen, L. Zheng, Z. Xu, A. Zhang, *J. Phys. D: Appl. Phys.* **2014**, *47*, 425103.
[33] Y. Z. Cheng, W. Withayachumnankul, A. Upadhyay, D. Headland, Y. Nie, R. Z. Gong, M. Bhaskaran, S. Sriram, D. Abbott, *Appl. Phys. Lett.* **2014**, *105*, 181111.
[34] S.-C. Jiang, X. Xiong, Y.-S. Hu, Y.-H. Hu, G.-B. Ma, R.-W. Peng, C. Sun, M. Wang, *Phys. Rev. X* **2014**, *4*, 021026.
[35] D. F. Pile, T. Ogawa, D. K. Gramotnev, Y. Matsuzaki, K. C. Vernon, K. Yamaguchi, T. Okamoto, M. Haraguchi, M. Fukui, *Appl. Phys. Lett.* **2005**, *87*, 261114.
[36] H. Choo, M. K. Kim, M. Staffaroni, T. J. Seok, J. Bokor, S. Cabrini, P. J. Schuck, M. C. Wu, E. Yablonovitch, *Nat. Photonics* **2012**, *6*, 838.
[37] S. Sun, K.-Y. Yang, C.-M. Wang, T.-K. Juan, W. T. Chen, C. Y. Liao, Q. He, S. Xiao, W.-T. Kung, G.-Y. Guo, L. Zhou, D. P. Tsai, *Nano Lett.* **2012**, *12*, 6223.
[38] A. Pors, M. G. Nielsen, R. L. Eriksen, S. I. Bozhevolnyi, *Nano Lett.* **2013**, *13*, 829.
[39] A. Pors, O. Albrektsen, I. P. Radko, S. I. Bozhevolnyi, *Sci. Rep.* **2013**, *3*, 2155.
[40] A. Pors, M. G. Nielsen, S. I. Bozhevolnyi, *Opt. Lett.* **2013**, *38*, 513.
[41] Y. Dai, W. Ren, H. Cai, H. Ding, N. Pan, X. Wang, *Opt. Express* **2014**, *22*, 7465.
[42] M. Farmahini-Farahani, H. Mosallaei, *Opt. Lett.* **2013**, *38*, 462.
[43] T. Niu, W. Withayachumnankul, A. Upadhyay, P. Gutruf, D. Abbott, M. Bhaskaran, S. Sriram, C. Fumeaux, *Opt. Express* **2014**, *22*, 16148.
[44] Y. Yifat, M. Eitan, Z. Iluz, Y. Hanein, A. Boag, J. Scheuer, *Nano Lett.* **2014**, *14*, 2485.
[45] Y. Yang, W. Wang, P. Moitra, I. I. Kravchenko, D. P. Briggs, J. Valentine, *Nano Lett.* **2014**, *14*, 1394.
[46] Q. Zhao, J. Zhou, F. Zhang, D. Lippens, *Mater. Today* **2009**, *12*, 60.
[47] D. Lin, P. Fan, E. Hasman, M. L. Brongersma, *Science* **2014**, *345*, 298.
[48] Y. Yao, R. Shankar, M. A. Kats, Y. Song, J. Kong, M. Loncar, F. Capasso, *Nano Lett.* **2014**, *14*, 6526.
[49] H. Cheng, S. Chen, P. Yu, J. Li, B. Xie, Z. Li, J. Tian, *Appl. Phys. Lett.* **2013**, *103*, 223102.
[50] C. Pfeiffer, N. K. Emani, A. M. Shaltout, A. Boltasseva, V. M. Shalaev, A. Grbic, *Nano Lett.* **2014**, *14*, 2491.
[51] C. Pfeiffer, A. Grbic, *Phys. Rev. Lett.* **2013**, *110*, 197401.
[52] C. Pfeiffer, A. Grbic, *Appl. Phys. Lett.* **2013**, *102*, 231116.
[53] J. Li, S. Chen, H. Yang, J. Li, P. Yu, H. Cheng, C. Gu, H.-T. Chen, J. Tian. *Adv. Funct. Mater.* **2015**, *25*, 704.
[54] E. Verhagen, J. A. Dionne, L. Kuipers, H. A. Atwater, A. Polman, *Nano Lett.* **2008**, *8*, 2925.
[55] J. Chen, G. A. Smolyakov, S. R. Brueck, K. J. Malloy, *Opt. Express* **2008**, *16*, 14902.
[56] F. Monticone, N. M. Estakhri, A. Alù, *Phys. Rev. Lett.* **2013**, *110*, 203903.
[57] N. Engheta, A. Salandrino, A. Alù, *Phys. Rev. Lett.* **2005**, *95*, 095504.
[58] A. Silva, F. Monticone, G. Castaldi, V. Galdi, A. Alù, N. Engheta, *Science* **2014**, *343*, 160.
[59] G. A. Siviloglou, N. C. Demetrios, *Opt. Lett.* **2007**, *32*, 979.
[60] G. A. Siviloglou, J. Broky, A. Dogariu, D. N. Christodoulides, *Phys. Rev. Lett.* **2007**, *99*, 213901.
[61] E. R. Dowski, W. T. Cathey, *Appl. Opt.* **1995**, *34*, 1859.
[62] C. D. Giovampaola, N. Engheta, *Nat. Mater.* **2014**, *13*, 1115.
[63] T. J. Cui, M. Q. Qi, X. Wan, J. Zhao, Q. Cheng, *Light Sci. Appl.* **2014**, *3*, e218.
[64] S. Zhang, F. Liu, T. Zentgraf, J. Li, *Phys. Rev. A* **2013**, *88*, 023823.
[65] C. Menzel, C. Helgert, C. Rockstuhl, E. B. Kley, A. Tünnermann, T. Pertsch, F. Lederer, *Phys. Rev. Lett.* **2010**, *104*, 253902.

[66] C. Pfeiffer, C. Zhang, V. Ray, L. J. Guo, A. Grbic, *Phys. Rev. Lett.* **2014**, *113*, 023902.
[67] Y. Zhao, M. A. Belkin, A. Alù, *Nat. Commun.* **2012**, *3*, 870.
[68] J. H. Shi, H. F. Ma, C. Y. Guan, Z. P. Wang, T. J. Cui, *Phys. Rev. B* **2014**, *89*, 165128.
[69] Z. Li, S. Chen, C. Tang, W. Liu, H. Cheng, Z. Liu, J. Li, P. Yu, B. Xie, Z. Liu, J. Li, J. Tian, *Appl. Phys. Lett.* **2014**, *105*, 201103.
[70] J. E. Roy, L. Shafai, *IEEE Antennas Propag. Mag.* **1996**, *38*, 18.
[71] C. Pfeiffer, A. Grbic, *Phys. Rev. Appl.* **2014**, *2*, 044011.
[72] C. Pfeiffer, A. Grbic, *IEEE Trans. Microw. Theory Tech.* **2013**, *61*, 4407.
[73] J. K. Gansel, M. Thiel, M. S. Rill, M. Decker, K. Bade, V. Saile, G. V. Freymann, S. Linden, M. Wegener, *Science* **2009**, *325*, 1513.
[74] A. Christofi, N. Stefanou, *Phys. Rev. B* **2013**, *87*, 115125.
[75] J. K. Gansel, M. Wegener, S. Burger, S. Linden, *Opt. Express* **2010**, *18*, 1059.
[76] L. Cong, W. Cao, X. Zhang, Z. Tian, J. Gu, R. Singh, J. Han, W. Zhang, *Appl. Phys. Lett.* **2013**, *103*, 171107.
[77] X. Zhuang, Y. Mai, D. Wu, F. Zhang, X. Feng, *Adv. Mater.* **2015**, *27*, 403.
[78] J. Gu, W. Zhang, H. Su, T. Fan, S. Zhu, Q. Liu, D. Zhang, *Adv. Mater.* **2015**, *27*, 464.